

pubs.acs.org/cm Article

# **Electronic Properties and Phase Transition in the Kagome Metal** Yb<sub>0.5</sub>Co<sub>3</sub>Ge<sub>3</sub>

Yaojia Wang, Gregory T. McCandless, Xiaoping Wang, Kulatheepan Thanabalasingam, Heng Wu, Damian Bouwmeester, Herre S. J. van der Zant, Mazhar N. Ali,\* and Julia Y. Chan\*



Cite This: https://doi.org/10.1021/acs.chemmater.2c01309



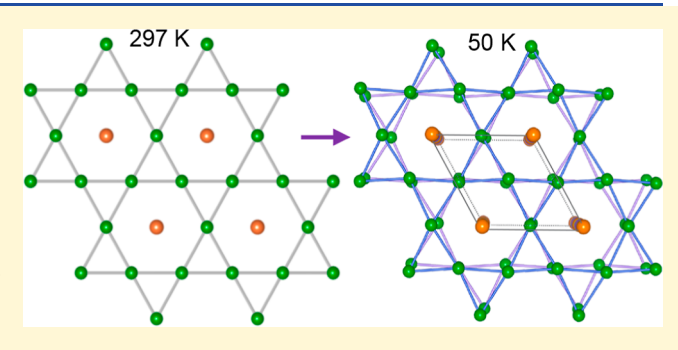
**ACCESS** I

Metrics & More

Article Recommendations

Supporting Information

ABSTRACT: The Kagome lattice is an important fundamental structure in condensed matter physics for investigating the interplay of electron correlation, topology, and frustrated magnetism. Recent work on Kagome metals in the AV<sub>3</sub>Sb<sub>5</sub> (A = K, Rb, and Cs) family has shown a multitude of correlation-driven distortions, including symmetry breaking charge density waves and nematic superconductivity at low temperatures. Here, we study the new Kagome metal Yb<sub>0.5</sub>Co<sub>3</sub>Ge<sub>3</sub> and find a temperature-dependent kink in the resistivity that is highly similar to the AV<sub>3</sub>Sb<sub>5</sub> behavior and is commensurate with an in-plane structural distortion of the Co Kagome lattice along with a doubling of the c-axis. The



symmetry is lower below the transition temperature, with a breaking the in-plane mirror planes and C<sub>6</sub> rotation, while gaining a screw axis along the c-direction. At very low temperatures, anisotropic negative magnetoresistance is observed, which may be related to anisotropic magnetism. This raises questions about the types of the distortions in Kagome nets and their resulting physical properties including superconductivity and magnetism.

#### INTRODUCTION

Materials containing 2D Kagome lattices, also known as trihexagonal tiling, are of extreme interest in condensed matter physics today. The Kagome lattice is made up of hexagons that are surrounded on their edges by equilateral triangles. Analogous to the honeycomb lattice, the Kagome lattice is an important structure for realizing a quantum spin liquid state due to its inherent geometric frustration; some of the leading spin liquid candidates are Kagome insulators. 1,2 Recently, however, Kagome metals have gained attention due to the realization of both topological Dirac electrons and flat bands and van Hove singularities resulting in strong electron correlation.<sup>3-7</sup> Materials in the AV<sub>3</sub>Sb<sub>5</sub> (A = K, Cs, and Rb) family<sup>8-11</sup> have shown both topological bands with low effective mass, a large anomalous Hall effect, 12,13 and a cascade of charge density wave (CDW)14-23 orderings and superconductivity<sup>24–30</sup> as temperature is lowered.

The intertwining of orders seen in Kagome metals is a complicated interplay of electronic correlation, topology, and magnetism, resulting in nearby ground states that are accessible by temperature control. While some phases (AV<sub>3</sub>Sb<sub>5</sub>) have shown electronic correlation-related charge orders and top-ology, others have shown topology and magnetism.<sup>31–39</sup> Studies are ongoing on Kagome systems which show correlation and magnetism, where charge/spin orders intertwine with magnetic orders of a spin sublattice. It has been shown that the structural distortions of the Kagome lattice and

symmetry breaking are closely related to the appearance of new orders, including the symmetry breaking CDW order observed in AV<sub>3</sub>Sb<sub>5</sub> compounds and antiferromagnetic FeGe. 40 How the various orders work together, or compete with each other, and what effect that has on structural distortions in the Kagome net and the resulting physical properties remain an active area of investigation.

In this paper, we report the presence of a kink in the resistivity at 95 K, below which there is a structural phase transition resulting in the distortion of the Co Kagome net, in the new Kagome metal Yb<sub>0.5</sub>Co<sub>3</sub>Ge<sub>3</sub>. Through single-crystal Xray diffraction structure determination, the low-temperature structure was found to break C<sub>6</sub> rotation symmetry and out-ofplane mirror planes, lowering symmetry from the P6/mmm space group to  $P6_3/m$ . In addition, a small upturn is evident in the resistivity below 18 K, commensurate with a previously seen transition in magnetization. Below this temperature, anisotropic negative magnetoresistance is observed, in contrast with the positive magnetoresistance seen in other Kagome metals such as AV<sub>3</sub>Sb<sub>5</sub>. Yb<sub>0.5</sub>Co<sub>3</sub>Ge<sub>3</sub> is a good platform for studying the effect of correlation and magnetism on the electronic properties in a Kagome system and adds to the

Received: April 30, 2022 Revised: July 19, 2022



ongoing effort to understand the phase space of Kagome metals.

#### ■ EXPERIMENTAL SECTION

**Synthesis and Property Measurements.** Single crystals of  $Yb_{0.5}Co_3Ge_3$  were grown as reported previously. Elements were weighed out into a Canfield crucible  $set^{42}$  with a molar ratio of 3:2:7:52 Yb/Co/Ge/Sn, respectively, and sealed in a fused silica tube filled with argon gas ~1/3 atm pressure. The sealed ampoule was then heated in a furnace to 1175 °C at 100 °C/h and dwelled for 24 h before cooling the ampoule down to 815 °C at a rate of 3 °C/h. The ampoule was then removed from the furnace, inverted, and centrifuged to remove the excess flux from the crystals. The needle-shaped crystals were then etched with dilute HCl followed by dilute HNO<sub>3</sub> etching to remove residual flux from the crystal surface. Silver paste was used to make contact with  $Yb_{0.5}Co_3Ge_3$  crystals, and the electrical properties were measured in a Quantum Design physical property measurement system (PPMS) using the four-probe method with an a.c. current applied along the c-axis.

Single-Crystal X-ray Diffraction. For comparison, the crystal structure of Yb<sub>0.5</sub>Co<sub>3</sub>Ge<sub>3</sub> collected at room temperature <sup>41</sup> is compared to the low-temperature model. The 50 K single-crystal X-ray diffraction data were collected using a Rigaku XtaLAB AFC12-(RCD3) diffractometer equipped with graphite monochromated Mo  $K\alpha$  radiation ( $\lambda = 0.71073$  Å), HyPix-6000He area detector, and Rigaku Oxford Diffraction CrysAlisPro software. Sample temperature was controlled with the dual flow nitrogen and helium gas cooler N-Helix by Oxford Cryosystems. The numerical absorption correction was completed based on Gaussian integration over a multifaceted crystal model. The empirical absorption correction was carried out using spherical harmonics implemented in the SCALE3 ABSPACK scaling algorithm in CrysAlis PRO 1.171.41.123a (Rigaku Oxford diffraction 2022). The 50 K data were modeled in Jana 2006 software 43 using the room temperature structure as the preliminary structural model. Table 1 provides the unit cell parameters and space group at room temperature and 50 K.

Table 1. Unit Cell Parameters from Single-Crystal X-ray Diffraction

	297 K	50 K
formula	$Yb_{0.5}Co_3Ge_3$	Yb <sub>0.5</sub> Co <sub>3</sub> Ge <sub>3</sub>
space group	P6/mmm	$P6_3/m$
lattice parameters		
a (Å)	5.0949(10)	5.0705(4)
c (Å)	3.9136(9)	7.7780(9)
V (Å <sup>3</sup> )	87.98(4)	173.18(3)
Z	1	2

#### ■ RESULTS AND DISCUSSION

 $Yb_{0.5}Co_3Ge_3$  crystallizes in the hexagonal P6/mmm space group at room temperature<sup>41</sup> and adopts a hybrid structure of the  $YCo_6Ge_6$  and CoSn prototypes<sup>44–46</sup> with a Co Kagome lattice; the crystal structure is shown in Figure 1a. The comparison between these structures is also included in the Supporting Information.

Single crystals of Yb<sub>0.5</sub>Co<sub>3</sub>Ge<sub>3</sub> present a rod-like shape with the long axis being the *c*-axis. <sup>41</sup> Figure 1b shows the temperature-dependent resistivity  $\rho(T)$  curve, which presents metallic behavior with reducing temperature. Several points of interest are observed on the  $\rho(T)$  curve; the first one is an evident kink near  $T^* \sim 95$  K with a clear transition on the  $d\rho(T)/dT$  versus T curve (lower inset Figure 1b). This is found to correspond to a structural phase transition, which will be discussed in detail below. Below  $\sim 18$  K, a weak upturn of

the resistivity is observed (also shown by the change in sign of the  $\mathrm{d}\rho(T)/\mathrm{d}T$  versus T curve in the inset), followed by a superconductor-like transition  $\sim\!3.6$  K (upper inset Figure 1b). Above the upturn of the resistivity, the low-temperature  $\rho(T)$  data (23–60 K) are well fitted using the equation  $\rho(T)=\rho(0)+AT^n$  (black line in Figure 1b), with n=2.04,  $\rho(0)\approx14.7~\mu\Omega$  cm, and  $A\approx0.00127~\mu\Omega$  cm K $^{-2}$ , suggesting that electronelectron interactions dominate electronic transport in this regime.  $^{34,47}$ 

The magnetoresistance is measured to study the magnetic response at low temperature. Figure 1c shows the  $\rho(H)$  data measured with magnetic field applied in the Kagome plane  $(H \perp I)$  and perpendicular to the Kagome plane (H/I) at 2 K. The rapid increase in  $\rho(H)$  at a very small field ( $\mu_0 H_c \sim 15 \text{ mT}$ for  $H \perp I$  and  $\mu_0 H_c \sim 20$  mT for H/I) confirms the superconducting transition. Since the resistivity does not reach zero (only an ~30% drop) and the superconducting signal is very close to the superconductivity of Sn ( $T_c \sim 3.72$  K and  $\mu_0 H_c \sim 30$  mT), it is likely that the superconductivity is not intrinsic but is rather coming from a Sn flux residual, although the sample was carefully centrifuged after growth and etched in dilute HCl and HNO3 to remove the residual of Sn flux. Investigation with doping and extremely low temperature study are necessary to search for superconductivity in this material, which is beyond the scope of this work.

After breaking superconductivity, a negative magnetoresistance is observed to high field, which is stronger for the magnetic field applied along the c-axis (H//I) compared with applying the magnetic field in the Kagome plane  $(H \perp I)$ . Figure 1d shows the temperature dependence of magnetoresistance measured with  $H \perp I$ , indicating that the negative magnetoresistance appears in the upturn region of resistivity (see Figure S2 for  $\rho$  vs T data in the Supporting Information). Kagome metals with weak magnetism typically present positive magnetoresistance, such as the AV<sub>3</sub>Sb<sub>5</sub> family, <sup>12,13</sup> and some CoSn-type materials.<sup>48</sup> Negative magnetoresistance has been seen in ferromagnetic Kagome materials and was also proposed to occur from electron correlation-induced ferromagnetic spin fluctuations.  $^{48,49}$  For  $Yb_{0.5}Co_3Ge_3$ , an earlier study on the magnetic behavior indicated that the compound has antiferromagnetic coupling without a clear long-range magnetic order. 41 In that study, below 15-20 K, a weak transition of magnetization was reported which was proposed to arise from spin canting or spin reorientation, and a larger magnetization was reported for the out-of-plane applied magnetic field (along the *c*-axis) compared with in the Kagome plane. The observed upturn of resistivity below 18–25 K in this work aligns very well with the temperature of the previously reported magnetization transition. These results indicate that the appearance of negative magnetoresistance is related to the magnetization transition, and the anisotropic negative magnetoresistance shown in Figure 1c may arise from the anisotropic magnetism in Yb<sub>0.5</sub>Co<sub>3</sub>Ge<sub>3</sub> at low temperature. Detailed study on the magnetic behavior of the phase in the future may reveal the origin of the transition and the negative magnetoresistance.

The main result of this work is the prominent transition near 95 K in the  $\rho(T)$ . Very similar transition features were observed in the  $\rho(T)$  of some Kagome metals, such as the  $AV_3Sb_5$  (A = K, Cs, and Rb) family and the antiferromagnetic Kagome metal FeGe, between 75 and 100 K. These transitions were found to be the result of superlattice formation from CDW ordering. To reveal whether there was a

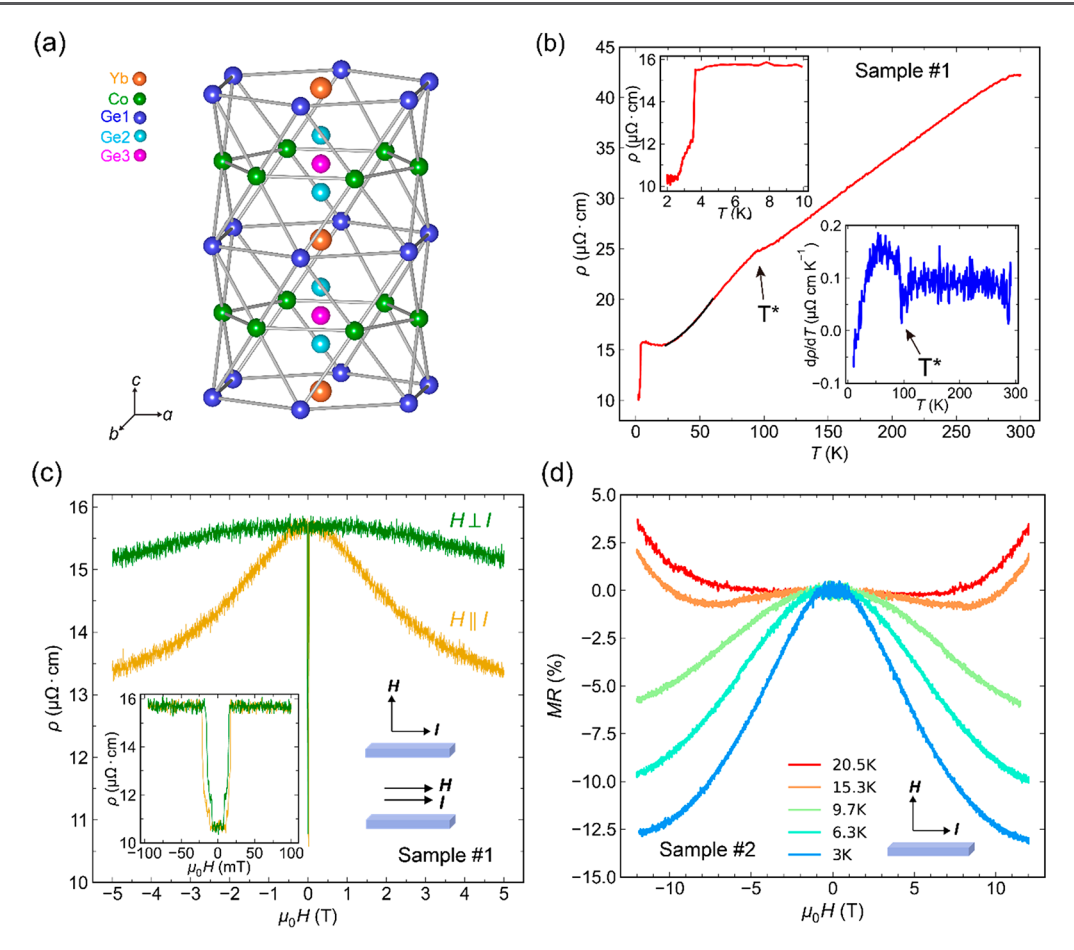


Figure 1. Structure and properties of  $Yb_{0.5}Co_3Ge_3$  (a). Crystal structure of  $Yb_{0.5}Co_3Ge_3$  in the P6/mmm phase. (b). Temperature dependence of the resistivity with current applied along the c-axis. The top inset is the  $\rho$  vs T curve at low temperature, and the bottom inset is the  $d\rho/dT$  vs T curve. The transition near 95 K is marked by a black arrow. The black line on the  $\rho$  vs T curve in the main panel is a fit to  $\rho(T) = \rho(0) + AT^n$ . (c). Magnetic field dependence of the resistivity measured at 2 K. The inset on the left is the zoom-in of the superconductivity at a small field. A schematic of the applied magnetic field direction for H/I and  $H \perp I$  is shown in the inset on the right. (d). Temperature dependence of magnetoresistance measured, and resistivity is shown in S12 for  $H \perp I$ .

corresponding structural transition in Yb<sub>0.5</sub>Co<sub>3</sub>Ge<sub>3</sub>, we performed single-crystal X-ray diffraction above and below the transition temperature. Figure 2a,b shows the projection of the X-ray diffraction pattern along the a-axis (b-c plane) and caxis (a-b plane) in reciprocal space, respectively. In the (0kl)plane (b-c) plane), a new set of diffraction peaks (marked by the orange box) can be seen in the 50 K pattern, located at half-integer spacing along the *l* direction (*c*-axis in real space, Figure 2a), compared with the diffraction pattern measured at room temperature. These new peaks arise from the formation of a superlattice with a doubled unit cell along the c-axis. In the (hk0) plane (a-b plane), a new set of diffraction peaks (marked by the yellow circles) is also observed at 50 K compared with the 297 K pattern (Figure 2b). These peaks do not arise from a superlattice formation in the a-b plane but instead become visible at 50 K due to distortion of the Kagome lattice.

The lattice parameters of  $Yb_{0.5}Co_3Ge_3$  obtained at 297 K and at 50 K from the single-crystal X-ray diffraction are provided in Table 1, and the corresponding crystal structure is shown in Figure 3. The crystal structure of  $Yb_{0.5}Co_3Ge_3$  can be described as a stacking of alternating subunits—a subunit with a hexagonal array (or honeycomb arrangement) of Ge atoms that can be partially stuffed in-plane with Yb and the transition metal (Co) Kagome net that contains Ge atoms within the

hexagons which can be displaced out-of-plane in response to partial occupation of the Yb above or below them (Figure 3a,b). The spacing between the planes of these subunits along the c-axis is  $\sim 1.96$  Å at room temperature and  $\sim 1.94$  Å at 50 K, a relatively insignificant contraction along the c-axis. At room temperature, the tiling of hexagons and triangles in the Kagome net adopts ideal internal bond angles of 120 and  $60^\circ$ , respectively, with both types of geometric arrangements containing a uniform Co–Co interatomic distance of  $\sim 2.55$  Å, being a perfect Kagome net, as shown in Figure 3c.

At low temperature, the crystal structure of Yb<sub>0.5</sub>Co<sub>3</sub>Ge<sub>3</sub> is best modeled in the  $P6_3/m$  space group due to a geometric distortion within the plane of the Kagome net. This is not driven by either the Yb or Ge atoms, which retain their geometric relations very closely with the room temperature structure, but rather from the deviation of the Co atoms from the ideal positions of the Kagome lattice. The triangular arrangements remain unaltered (or temperature-independent) in their interatomic distances but are slightly rotated relative to each other (Figure 3d), resulting in the hexagonal arrangements becoming distorted. The bond angles in the hexagons therefore deviate by  $\pm \sim 7.5^{\circ}$  from the ideal internal bond angles of 120° in an alternating fashion when comparing angles between the edges at neighboring vertices of the hexagons. This results in a deformation of the Kagome net, a twisting of

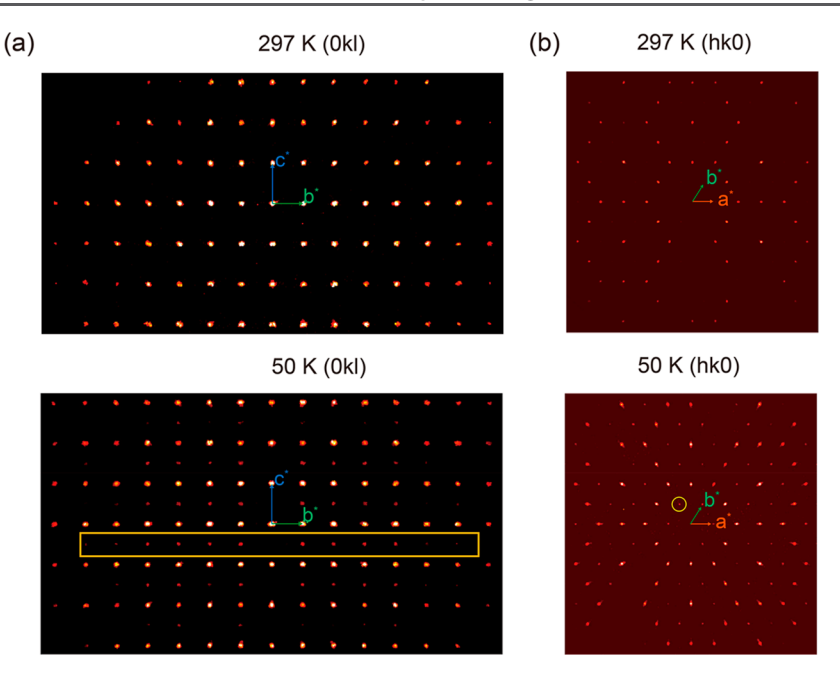


**Figure 2.** X-ray diffraction pattern. (a) Projection of the diffraction pattern along the *a*-axis (0*kl* plane) at 297 and 50 K. The appearance of superlattice peaks (marked by the orange rectangle) at 50 K is due to the doubling of the *c*-axis. (b) Projection of the diffraction pattern along the *c*-axis (*hk*0 plane) at 297 and 50 K. The new peaks (marked by the yellow circle) appearing at 50 K become visible due to the distortion of the Co lattice.

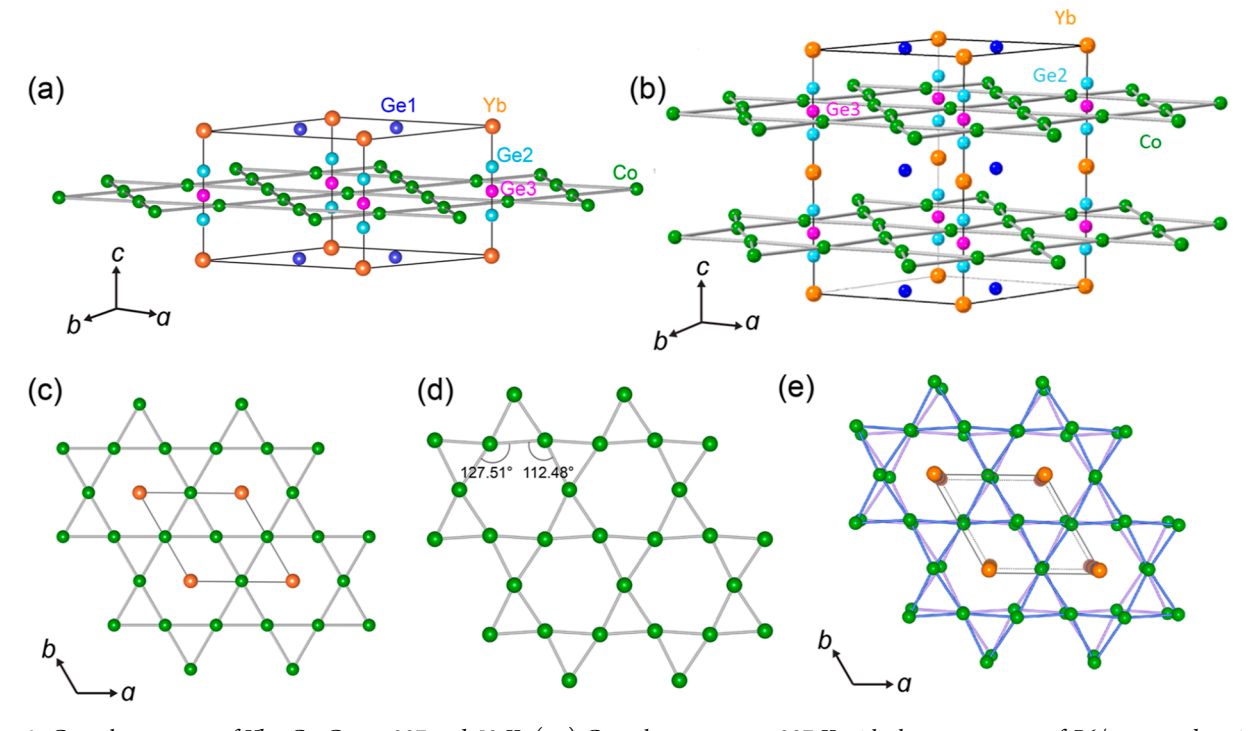


Figure 3. Crystal structures of  $Yb_{0.5}Co_3Ge_3$  at 297 and 50 K. (a,c) Crystal structures at 297 K with the space group of P6/mmm and projection down the c-direction of the Co Kagome network. (b) Crystal structure at 50 K with the space group of  $P6_3/m$ . (d) Distortion of one of the Co Kagome layers at 50 K with the modified bond angles of the hexagons labeled. (e) Two layers of the distorted Co Kagome layers unit cell showcasing their rotation relative to each other.

the triangular units with respect to each other that breaks  $C_6$  rotational and inversion symmetry, and results in the loss of all mirror planes parallel to the *c*-axis, subsequently reducing the space group to  $P6_3/m$  from the original P6/mmm. Additionally, the geometric distortion of the Kagome subunit changes the long-range ordering along the *c*-axis. At room temperature, the unit cell is defined with the shorter *c*-axis ( $c \sim 3.91 \text{ Å}$ ) and one

Kagome subunit located at z=1/2. At T=50 K, the long-range ordering along the c-axis requires a doubling ( $c\sim7.78$  Å) and the unit cell now contains two Kagome subunits located at z=1/4 and 3/4 (Figure 3b,e). These are related to each other by a sixfold screw axis along c, and an inversion center is located between the Kagome nets, making the full structure centrosymmetric, even though a single distorted

Kagome net breaks inversion symmetry (Figure 3d). The distorted Kagome net at low temperature is distinct from AV<sub>3</sub>Sb<sub>5</sub> family, <sup>19,23</sup> a similar distortion has been seen in the Kagome metals MgCo<sub>6</sub>Ge<sub>6</sub>, 50 LaRu<sub>3</sub>Si<sub>2</sub>, and YRu<sub>3</sub>Si<sub>2</sub>, and some of the phases are superconductors but show no sign of magnetic or  $\overline{\text{CDW}}$  transitions above  $T_{\text{c}}^{-51-55}$  It is worth noting that although a magnetic transition at low temperature (18 K) was detected in the previous magnetic susceptibility study, no magnetic transition signal was observed between 50 and 300 K.<sup>41</sup> This may be related to the distortion of the Co Kagome nets, which is inverted between the two layers and may influence magnetization; future experiments such a muon spin relaxation may help to explicitly understand the magnetism and its relation to the resistive transition in Yb<sub>0.5</sub>Co<sub>3</sub>Ge<sub>3</sub>. The feature of a resistive transition arising from a CDW but without an associated magnetic signal has been observed in other materials.56,57

In summary, we investigated the crystal structure and transport properties of the Kagome metal Yb<sub>0.5</sub>Co<sub>3</sub>Ge<sub>3</sub> and found a symmetry lowering structural phase transition around 95 K commensurate with a kink in the resistivity that is very similar to the CDW transition found in the AV<sub>3</sub>Sb<sub>5</sub> and FeGe Kagome metals. Based on our measurements down to 2 K, we do not find intrinsic superconductivity; however, we do observe anisotropic negative magnetoresistance that correlates with previous study on a magnetic transition around 18 K. The 95 K transition distorts the Kagome net, keeping the triangular units consistent but rotating them slightly relative to each other, breaking C<sub>6</sub> rotation, out-of-plane mirror, and inversion symmetry. Since it is known that the structure of the Kagome lattice drives flat bands, Dirac bands, and magnetic frustration in Kagome metals, resulting in strong electron correlation, topological electrons, and complex magnetic states, which significantly influences the electronic properties, Yb<sub>0.5</sub>Co<sub>3</sub>Ge<sub>3</sub> and its distortion merit further theoretical and experimental investigation. Angle-resolved photoemission spectroscopy with associated band structure calculations can be performed to understand the band structure modifications associated with the phase transition and correlations in this material. Of particular importance is determining whether the structural transition is associated with the formation of the CDW order in analogy to other Kagome metals, ideally studied using scanning tunneling microscopy (STM). As recently discovered in the AV<sub>3</sub>Sb<sub>5</sub> family, where multiple charge-ordered phases were found as a function of decreasing temperature via STM but were hidden in resistive transport measurements, there may be further orderings present in Yb<sub>0.5</sub>Co<sub>3</sub>Ge<sub>3</sub>, which remain to be found. Additionally, the magnetism in Yb<sub>0.5</sub>Co<sub>3</sub>Ge<sub>3</sub> at low temperature may also induce spin orders, and muon spin relaxation measurements could elucidate this. Finally, since superconductivity has been observed in some other materials with distorted Kagome lattices and nematic superconductivity in the AV<sub>3</sub>Sb<sub>5</sub> family, further studies based on chemical doping or high-pressure approaches at lower temperature can be used in Yb<sub>0.5</sub>Co<sub>3</sub>Ge<sub>3</sub> to probe this and its potential relation to the structural transition.

#### ASSOCIATED CONTENT

#### Supporting Information

The Supporting Information is available free of charge at https://pubs.acs.org/doi/10.1021/acs.chemmater.2c01309.

CoSn and  $HfFe_6Ge_6$  structure types and temperature dependence of resistivity of an additional sample with and without the field (PDF)

Yb<sub>0.5</sub>Co<sub>3</sub>Ge<sub>3</sub> at 50K (CIF)

#### AUTHOR INFORMATION

## **Corresponding Authors**

Mazhar N. Ali — Kavli Institute of Nanoscience, Delft University of Technology, 2628 CJ Delft, The Netherlands; Department of Quantum Nanoscience, Faculty of Applied Sciences, Delft University of Technology, 2628 CJ Delft, The Netherlands; Email: M.N.Ali@tudelft.nl

Julia Y. Chan — Department of Chemistry and Biochemistry, Baylor University, Waco, Texas 76798, United States; orcid.org/0000-0003-4434-2160; Email: Julia\_Chan@baylor.edu

#### **Authors**

Yaojia Wang — Kavli Institute of Nanoscience, Delft University of Technology, 2628 CJ Delft, The Netherlands; Department of Quantum Nanoscience, Faculty of Applied Sciences, Delft University of Technology, 2628 CJ Delft, The Netherlands

Gregory T. McCandless – Department of Chemistry and Biochemistry, Baylor University, Waco, Texas 76798, United States

Xiaoping Wang — Neutron Scattering Division, Oak Ridge National Laboratory, Oak Ridge, Tennessee 37831, United States; Oorcid.org/0000-0001-7143-8112

Kulatheepan Thanabalasingam – Department of Chemistry and Biochemistry, Baylor University, Waco, Texas 76798, United States

Heng Wu – Kavli Institute of Nanoscience, Delft University of Technology, 2628 CJ Delft, The Netherlands; Department of Quantum Nanoscience, Faculty of Applied Sciences, Delft University of Technology, 2628 CJ Delft, The Netherlands

Damian Bouwmeester – Kavli Institute of Nanoscience, Delft University of Technology, 2628 CJ Delft, The Netherlands; Department of Quantum Nanoscience, Faculty of Applied Sciences, Delft University of Technology, 2628 CJ Delft, The Netherlands

Herre S. J. van der Zant – Kavli Institute of Nanoscience, Delft University of Technology, 2628 CJ Delft, The Netherlands; Department of Quantum Nanoscience, Faculty of Applied Sciences, Delft University of Technology, 2628 CJ Delft, The Netherlands; orcid.org/0000-0002-5385-0282

Complete contact information is available at: https://pubs.acs.org/10.1021/acs.chemmater.2c01309

### Notes

The authors declare no competing financial interest.

# ACKNOWLEDGMENTS

Y.W. acknowledges the support from NWO Talent Program Veni financed by the Dutch Research Council (NWO), project no. VI.Veni.212.146. A portion of this research used resources at the Spallation Neutron Source, a Department of Energy Office of Science User Facility operated by the Oak Ridge National Laboratory. J.Y.C. acknowledges NSF-DMR 2209804 and Welch AT-2056-20210327 for partial support of this work. M.N.A. acknowledges support from the Kavli Institute of Nanoscience Delft and the Faculty of Applied Sciences at TU Delft and the Max Planck Institute for Microstructure Physics

Halle. A portion of this research was supported by the Netherlands Organisation for Scientific Research (NWO/OCW), as part of the Frontiers of Nanoscience program.

#### REFERENCES

- (1) Balents, L. Spin Liquids in Frustrated Magnets. *Nature* 2010, 464, 199-208.
- (2) Zhou, Y.; Kanoda, K.; Ng, T. K. Quantum Spin Liquid States. *Rev. Mod. Phys.* **2017**, *89*, 025003.
- (3) Yu, S. L.; Li, J. X. Chiral Superconducting Phase and Chiral Spin-Density-Wave Phase in a Hubbard Model on the Kagome Lattice. *Phys. Rev. B: Condens. Matter Mater. Phys.* **2012**, *85*, 144402.
- (4) Kiesel, M. L.; Platt, C.; Thomale, R. Unconventional Fermi Surface Instabilities in the Kagome Hubbard Model. *Phys. Rev. Lett.* **2013**, *110*, 126405.
- (5) Kiesel, M. L.; Thomale, R. Sublattice Interference in the Kagome Hubbard Model. *Phys. Rev. B: Condens. Matter Mater. Phys.* **2012**, *86*, 121105.
- (6) Lin, Y. P.; Nandkishore, R. M. Complex Charge Density Waves at Van Hove Singularity on Hexagonal Lattices: Haldane-Model Phase Diagram and Potential Realization in the Kagome Metals (=K, Rb, Cs). *Phys. Rev. B* **2021**, *104*, 045122.
- (7) Wang, W.; Li, Z.; Xiang, Y.; Wang, Q. Competing Electronic Orders on Kagome Lattices at van Hove Filling. *Phys. Rev. B: Condens. Matter Mater. Phys.* **2013**, 87, 115135.
- (8) Ortiz, B. R.; Gomes, L. C.; Morey, J. R.; Winiarski, M.; Bordelon, M.; Mangum, J. S.; Oswald, I. W. H.; Rodriguez-Rivera, J. A.; Neilson, J. R.; Wilson, S. D.; Ertekin, E.; McQueen, T. M.; Toberer, E. S. New Kagome Prototype Materials: Discovery of KV<sub>3</sub>Sb<sub>5</sub>, RbV<sub>3</sub>Sb<sub>5</sub>, and CsV<sub>3</sub>Sb<sub>5</sub>. *Phys. Rev. Mater.* **2019**, *3*, 094407.
- (9) Neupert, T.; Denner, M. M.; Yin, J.-X.; Thomale, R.; Hasan, M. Z. Charge Order and Superconductivity in Kagome Materials. *Nat. Phys.* **2022**, *18*, 137–143.
- (10) Nguyen, T.; Li, M. Electronic properties of correlated kagomé metals  $AV_3Sb_5$  (A = K, Rb, and Cs): A perspective. *J. Appl. Phys.* **2022**, 131, 060901.
- (11) Jiang, K.; Wu, T.; Yin, J.; Wang, Z.; Hasan, M. Z.; Wilson, S. D.; Chen, X.; Hu, J. Kagome Superconductors  $AV_3Sb_5$  (A=K, Rb, Cs). **2021**, arXiv:2109.10809.
- (12) Yang, S. Y.; Wang, Y.; Ortiz, B. R.; Liu, D.; Gayles, J.; Derunova, E.; Gonzalez-Hernandez, R.; Šmejkal, L.; Chen, Y.; Parkin, S. S. P.; Wilson, S. D.; Toberer, E. S.; McQueen, T.; Ali, M. N. Giant, Unconventional Anomalous Hall Effect in the Metallic Frustrated Magnet Candidate KV<sub>3</sub>Sb<sub>5</sub>. Sci. Adv. 2020, 6, No. eabb6003.
- (13) Yu, F. H.; Wu, T.; Wang, Z. Y.; Lei, B.; Zhuo, W. Z.; Ying, J. J.; Chen, X. H. Concurrence of Anomalous Hall Effect and Charge Density Wave in a Superconducting Topological Kagome Metal. *Phys. Rev. B* **2021**, *104*, L041103.
- (14) Wang, Z.; Jiang, Y. X.; Yin, J. X.; Li, Y.; Wang, G. Y.; Huang, H. L.; Shao, S.; Liu, J.; Zhu, P.; Shumiya, N.; Hossain, M. S.; Liu, H.; Shi, Y.; Duan, J.; Li, X.; Chang, G.; Dai, P.; Ye, Z.; Xu, G.; Wang, Y.; Zheng, H.; Jia, J.; Hasan, M. Z.; Yao, Y. Electronic Nature of Chiral Charge Order in the Kagome Superconductor CsV<sub>3</sub>Sb<sub>5</sub>. *Phys. Rev. B* **2021**, *104*, 075148.
- (15) Zhao, H.; Li, H.; Ortiz, B. R.; Teicher, S. M. L.; Park, T.; Ye, M.; Wang, Z.; Balents, L.; Wilson, S. D.; Zeljkovic, I. Cascade of Correlated Electron States in the Kagome Superconductor CsV<sub>3</sub>Sb<sub>5</sub>. *Nature* **2021**, *599*, 216–221.
- (16) Jiang, Y. X.; Yin, J. X.; Denner, M. M.; Shumiya, N.; Ortiz, B. R.; Xu, G.; Guguchia, Z.; He, J.; Hossain, M. S.; Liu, X.; Ruff, J.; Kautzsch, L.; Zhang, S. S.; Chang, G.; Belopolski, I.; Zhang, Q.; Cochran, T. A.; Multer, D.; Litskevich, M.; Cheng, Z. J.; Yang, X. P.; Wang, Z.; Thomale, R.; Neupert, T.; Wilson, S. D.; Hasan, M. Z. Unconventional Chiral Charge Order in Kagome Superconductor KV<sub>3</sub>Sb<sub>5</sub>. Nat. Mater. 2021, 20, 1353–1357.
- (17) Chen, H.; Yang, H.; Hu, B.; Zhao, Z.; Yuan, J.; Xing, Y.; Qian, G.; Huang, Z.; Li, G.; Ye, Y.; Ma, S.; Ni, S.; Zhang, H.; Yin, Q.; Gong, C.; Tu, Z.; Lei, H.; Tan, H.; Zhou, S.; Shen, C.; Dong, X.; Yan, B.;

- Wang, Z.; Gao, H. J. Roton Pair Density Wave in a Strong-Coupling Kagome Superconductor. *Nature* **2021**, *599*, 222–228.
- (18) Nie, L.; Sun, K.; Ma, W.; Song, D.; Zheng, L.; Liang, Z.; Wu, P.; Yu, F.; Li, J.; Shan, M.; Zhao, D.; Li, S.; Kang, B.; Wu, Z.; Zhou, Y.; Liu, K.; Xiang, Z.; Ying, J.; Wang, Z.; Wu, T.; Chen, X. Charge-Density-Wave-Driven Electronic Nematicity in a Kagome Superconductor. *Nature* 2022, 604, 59–64.
- (19) Ortiz, B. R.; Teicher, S. M. L.; Kautzsch, L.; Sarte, P. M.; Ratcliff, N.; Harter, J.; Ruff, J. P. C.; Seshadri, R.; Wilson, S. D. Fermi Surface Mapping and the Nature of Charge-Density-Wave Order in the Kagome Superconductor CsV<sub>3</sub>Sb<sub>5</sub>. *Phys. Rev. X* **2021**, *11*, 041030.
- (20) Denner, M. M.; Thomale, R.; Neupert, T. Analysis of Charge Order in the Kagome Metal  $AV_3Sb_5$  (A= K,Rb,Cs). *Phys. Rev. Lett.* **2021**, 127, 217601.
- (21) Subedi, A. Hexagonal-to-Base-Centered-Orthorhombic 4Q Charge Density Wave Order in Kagome Metals KV<sub>3</sub>Sb<sub>5</sub>, RbV<sub>3</sub>Sb<sub>5</sub>, and CsV<sub>2</sub>Sb<sub>5</sub> Alaska. *Phys. Rev. Mater.* **2022**, *6*, 015001.
- (22) Feng, X.; Jiang, K.; Wang, Z.; Hu, J. Chiral Flux Phase in the Kagome Superconductor AV<sub>3</sub>Sb<sub>5</sub>. Sci. Bull. **2021**, 66, 1384–1388.
- (23) Stahl, Q.; Chen, D.; Ritschel, T.; Shekhar, C.; Sadrollahi, E.; Rahn, M. C.; Ivashko, O.; Zimmermann, M. V.; Felser, C.; Geck, J. Temperature-Driven Reorganization of Electronic Order in CsV<sub>3</sub>Sb<sub>5</sub>. *Phys. Rev. B* **2022**, *105*, 195136.
- (24) Xiang, Y.; Li, Q.; Li, Y.; Xie, W.; Yang, H.; Wang, Z.; Yao, Y.; Wen, H. H. Twofold Symmetry of c-Axis Resistivity in Topological Kagome Superconductor CsV<sub>3</sub>Sb<sub>5</sub> with in-Plane Rotating Magnetic Field. *Nat. Commun.* **2021**, *12*, *6727*.
- (25) Ortiz, B. R.; Teicher, S. M. L.; Hu, Y.; Zuo, J. L.; Sarte, P. M.; Schueller, E. C.; Abeykoon, A. M. M.; Krogstad, M. J.; Rosenkranz, S.; Osborn, R.; Seshadri, R.; Balents, L.; He, J.; Wilson, S. D. CsV<sub>3</sub>Sb<sub>5</sub>: A Z2 Topological Kagome Metal with a Superconducting Ground State. *Phys. Rev. Lett.* **2020**, *125*, 247002.
- (26) Ortiz, B. R.; Sarte, P. M.; Kenney, E. M.; Graf, M. J.; Teicher, S. M. L.; Seshadri, R.; Wilson, S. D. Superconductivity in the Z<sub>2</sub> Kagome Metal KV<sub>3</sub>Sb<sub>5</sub>. *Phys. Rev. Mater.* **2021**, *5*, 034801.
- (27) Chen, K. Y.; Wang, N. N.; Yin, Q. W.; Gu, Y. H.; Jiang, K.; Tu, Z. J.; Gong, C. S.; Uwatoko, Y.; Sun, J. P.; Lei, H. C.; Hu, J. P.; Cheng, J. G. Double Superconducting Dome and Triple Enhancement of Tc in the Kagome Superconductor CsV<sub>3</sub>Sb<sub>5</sub> under High Pressure. *Phys. Rev. Lett.* **2021**, *126*, 247001.
- (28) Xu, H.; Yan, Y.; Yin, R.; Xia, W.; Fang, S.; Chen, Z.; Li, Y.; Yang, W.; Guo, Y.; Feng, D. Multiband Superconductivity with Sign-Preserving Order Parameter in Kagome Superconductor CsV<sub>3</sub>Sb<sub>5</sub>. *Phys. Rev. Lett.* **2021**, *127*, 187004.
- (29) Yu, F. H.; Ma, D. H.; Zhuo, W. Z.; Liu, S. Q.; Wen, X. K.; Lei, B.; Ying, J. J.; Chen, X. H. Unusual Competition of Superconductivity and Charge-Density-Wave State in a Compressed Topological Kagome Metal. *Nat. Commun.* **2021**, *12*, 3645.
- (30) Wang, Y.; Yang, S. Y.; Sivakumar, P. K.; Ortiz, B. R.; Teicher, S. M. L.; Wu, H.; Srivastava, A. K.; Garg, C.; Liu, D.; Parkin, S. S. P.; Toberer, E. S.; McQueen, T.; Wilson, S. D.; Ali, M. N. Proximity-Induced Spin-Triplet Superconductivity and Edge Supercurrent in the Topological Kagome Metal,  $K_{1-x}V_3Sb_5$ . **2020**, arXiv:2012.05898.
- (31) O'Neill, C. D.; Wills, A. S.; Huxley, A. D. Possible Topological Contribution to the Anomalous Hall Effect of the Noncollinear Ferromagnet Fe<sub>3</sub>Sn<sub>2</sub>. *Phys. Rev. B* **2019**, *100*, 174420.
- (32) Xu, T.; Chen, Z.; Zhou, H. A.; Wang, Z.; Dong, Y.; Aballe, L.; Foerster, M.; Gargiani, P.; Valvidares, M.; Bracher, D. M.; Savchenko, T.; Kleibert, A.; Tomasello, R.; Finocchio, G.; Je, S. G.; Im, M. Y.; Muller, D. A.; Jiang, W. Imaging the Spin Chirality of Ferrimagnetic Néel Skyrmions Stabilized on Topological Antiferromagnetic Mn<sub>3</sub>Sn. *Phys. Rev. Mater.* **2021**, *5*, 084406.
- (33) Kang, M.; Ye, L.; Fang, S.; You, J. S.; Levitan, A.; Han, M.; Facio, J. I.; Jozwiak, C.; Bostwick, A.; Rotenberg, E.; Chan, M. K.; McDonald, R. D.; Graf, D.; Kaznatcheev, K.; Vescovo, E.; Bell, D. C.; Kaxiras, E.; van den Brink, J.; Richter, M.; Prasad Ghimire, M.; Checkelsky, J. G.; Comin, R. Dirac Fermions and Flat Bands in the Ideal Kagome Metal FeSn. *Nat. Mater.* 2020, *19*, 163–169.

- (34) Pokharel, G.; Teicher, S. M. L.; Ortiz, B. R.; Sarte, P. M.; Wu, G.; Peng, S.; He, J.; Seshadri, R.; Wilson, S. D. Electronic Properties of the Topological Kagome Metals YV<sub>6</sub>Sn<sub>6</sub> and GdV<sub>6</sub>Sn<sub>6</sub>. *Phys. Rev. B* **2021**, *104*, 235139.
- (35) Rout, P. K.; Madduri, P. V. P.; Manna, S. K.; Nayak, A. K. Field-Induced Topological Hall Effect in the Noncoplanar Triangular Antiferromagnetic Geometry of Mn<sub>3</sub>Sn. *Phys. Rev. B* **2019**, *99*, 094430.
- (36) Ghimire, N. J.; Dally, R. L.; Poudel, L.; Jones, D. C.; Michel, D.; Magar, N.; Bleuel, M.; McGuire, M. A.; Jiang, J. S.; Mitchell, J. F.; Lynn, J. W.; Mazin, I. I. Competing Magnetic Phases and Fluctuation-Driven Scalar Spin Chirality in the Kagome Metal YMn<sub>6</sub>Sn<sub>6</sub>. *Sci. Adv.* **2020**, *6*, No. eabe2680.
- (37) Asaba, T.; Thomas, S. M.; Curtis, M.; Thompson, J. D.; Bauer, E. D.; Ronning, F. Anomalous Hall Effect in the Kagome Ferrimagnet GdMn<sub>6</sub>Sn<sub>6</sub>. *Phys. Rev. B* **2020**, *101*, 174415.
- (38) Lee, Y.; Skomski, R.; Wang, X.; Orth, P. P.; Pathak, A. K.; Harmon, B. N.; McQueeney, R. J.; Ke, L. Interplay between Magnetism and Band Topology in Kagome Magnets RMn<sub>6</sub>Sn<sub>6</sub>. **2022**, arXiv:2201.11265.
- (39) Ma, W.; Xu, X.; Yin, J. X.; Yang, H.; Zhou, H.; Cheng, Z. J.; Huang, Y.; Qu, Z.; Wang, F.; Hasan, M. Z.; Jia, S. Rare Earth Engineering in  $RMn_6Sn_6$  (R=Gd-Tm, Lu) Topological Kagome Magnets. *Phys. Rev. Lett.* **2021**, *126*, 246602.
- (40) Teng, X.; Chen, L.; Ye, F.; Rosenberg, E.; Liu, Z.; Yin, J.; Jiang, Y.-X.; Oh, J. S.; Hasan, M. Z.; Neubauer, K. J.; Gao, B.; Xie, Y.; Hashimoto, M.; Lu, D.; Jozwiak, C.; Bostwick, A.; Rotenberg, E.; Birgeneau, R. J.; Chu, J.-H.; Yi, M.; Dai, P. Discovery of Charge Density Wave in a Correlated Kagome Lattice Antiferromagnet. 2022, arXiv:2203.11467.
- (41) Weiland, A.; Eddy, L. J.; McCandless, G. T.; Hodovanets, H.; Paglione, J.; Chan, J. Y. Refine Intervention: Characterizing Disordered Yb<sub>0.5</sub>Co<sub>3</sub>Ge<sub>3</sub>. Cryst. Growth Des. **2020**, 20, 6715–6721.
- (42) Canfield, P. C.; Kong, T.; Kaluarachchi, U. S.; Jo, N. H. Use of Frit-Disc Crucibles for Routine and Exploratory Solution Growth of Single Crystalline Samples. *Philos. Mag.* **2016**, *96*, 84–92.
- (43) Petrícek, V.; Dušek, M.; Palatinus, L. Crystallographic Computing System JANA2006: General Features. *Z. Kristallogr.* **2014**, 229, 345–352.
- (44) Huang, H.; Zheng, L.; Lin, Z.; Guo, X.; Wang, S.; Zhang, S.; Zhang, C.; Sun, Z.; Wang, Z.; Weng, H.; Li, L.; Wu, T.; Chen, X.; Zeng, C. Flat-Band-Induced Anomalous Anisotropic Charge Transport and Orbital Magnetism in Kagome Metal CoSn. *Phys. Rev. Lett.* **2022**, *128*, 096601.
- (45) Meier, W. R.; Du, M. H.; Okamoto, S.; Mohanta, N.; May, A. F.; McGuire, M. A.; Bridges, C. A.; Samolyuk, G. D.; Sales, B. C. Flat Bands in the CoSn-Type Compounds. *Phys. Rev. B* **2020**, *102*, 075148.
- (46) Nial, O. X-Ray Examination of Cobalt-Tin Alloys and a Comparison of the System Co-Sn with Fe-Sn and Ni-Sn. *Z. Anorg. Allg. Chem.* **1938**, 238, 287–296.
- (47) Gui, X.; Cava, R. J. LaIr<sub>3</sub>Ga<sub>2</sub>: A Superconductor Based on a Kagome Lattice of Ir. **2021**, arXiv:2111.01247 2021.
- (48) Zhang, J.; Yilmaz, T.; Meier, J. W. R.; Pai, J. Y.; Lapano, J.; Li, H. X.; Kaznatcheev, K.; Vescovo, E.; Huon, A.; Brahlek, M.; Ward, T. Z.; Lawrie, B.; Moore, R. G.; Lee, H. N.; Wang, Y. L.; Miao, H.; Sales, B. Flat Band Induced Negative Magnetoresistance in Multi-Orbital Kagome Metal. 2021, arXiv:2105.08888.
- (49) Arita, R.; Kuroki, K.; Aoki, H. Electron-Correlation-Originated Negative Magnetoresistance in a System Having a Partly Flat Band. *Phys. Rev. B: Condens. Matter Mater. Phys.* **2000**, *61*, 3207–3210.
- (50) Sinha, M.; Vivanco, H. K.; Wan, C.; Siegler, M. A.; Stewart, V. J.; Pogue, E. A.; Pressley, L. A.; Berry, T.; Wang, Z.; Johnson, I.; Chen, M.; Tran, T. T.; Phelan, W. A.; McQueen, T. M. Twisting of 2D Kagomé Sheets in Layered Intermetallics. *ACS Cent. Sci.* **2021**, *7*, 1381–1390.
- (51) Li, S.; Zeng, B.; Wan, X.; Tao, J.; Han, F.; Yang, H.; Wang, Z.; Wen, H. H. Anomalous Properties in the Normal and Super-

- conducting States of LaRu<sub>3</sub>Si<sub>2</sub>. Phys. Rev. B: Condens. Matter Mater. Phys. 2011, 84, 214527.
- (52) Li, B.; Li, S.; Wen, H. H. Chemical Doping Effect in the LaRu<sub>3</sub>Si<sub>2</sub> Superconductor with a Kagome Lattice. *Phys. Rev. B* **2016**, 94, 094523.
- (53) Kishimoto, Y.; Ohno, T.; Hihara, T.; Sumiyama, K.; Ghosh, G.; Gupta, L. C. Magnetic Susceptibility Study of LaRu<sub>3</sub>Si<sub>2</sub>. *J. Phys. Soc. Jpn.* **2002**, *71*, 2035–2038.
- (54) Mielke, C.; Qin, Y.; Yin, J. X.; Nakamura, H.; Das, D.; Guo, K.; Khasanov, R.; Chang, J.; Wang, Z. Q.; Jia, S.; Nakatsuji, S.; Amato, A.; Luetkens, H.; Xu, G.; Hasan, M. Z.; Guguchia, Z. Nodeless Kagome Superconductivity in LaRu<sub>3</sub>Si<sub>3</sub>. *Phys. Rev. Mater.* **2021**, *5*, 034803.
- (55) Gong, C.; Tian, S.; Tu, Z.; Yin, Q.; Fu, Y.; Luo, R.; Lei, H. Superconductivity in Kagome Metal YRu<sub>3</sub>Si<sub>2</sub> with Strong Electron Correlations. **2021**, arXiv:2109.1147 *Chinese Phys. Lett.* **2022**, 39, 087401
- (56) Kolincio, K. K.; Roman, M.; Winiarski, M. J.; Strychalska-Nowak, J.; Klimczuk, T. Magnetism and Charge Density Waves in RNiC<sub>2</sub> (R=Ce, Pr, Nd). *Phys. Rev. B* **2017**, *95*, 235156.
- (57) Lei, H.; Wang, K.; Petrovic, C. Magnetic-Field-Tuned Charge Density Wave in SmNiC<sub>2</sub> and NdNiC<sub>2</sub>. *J. Phys.: Condens. Matter* **2017**, 29, 075602.